Infrared reflectivity versus doping in $YBa_2Cu_3O_{6+x}$ and $Nd_{1+y}Ba_{2-y}Cu_3O_{6+x}$ ceramics: Relationship with the t-J model

J. Bouvier and N. Bontemps*
Laboratoire d'Optique Physique, Ecole Supérieure de Physique et de Chimie Industrielles, 10 rue Vauquelin, 75231 Paris CEDEX 05, France

M. Gabay
Laboratoire de Physique des Solides, Université Paris–Sud, 91405, Orsay, France

M. Nanot and F. Queyroux
Laboratoire des Céramiques et Matériaux Minéraux, Ecole Supérieure de Physique et de Chimie Industrielles, 10 rue Vauquelin, 75231 Paris CEDEX 05, France
(Received 23 July 1991)

We have measured the room-temperature reflectivity spectra in the infrared and visible range (500–25 000 cm^{-1}) of $YBa_2Cu_3O_{6+x}$ ($0 \le x \le 1$) and $Nd_{1+y}Ba_{2-y}Cu_3O_{6+x}$ ($0 \le y \le 0.5$) polished ceramics as a function of doping (x and y). We show that the intensity of the entire infrared spectrum increases with the hole doping level (x or y). When separated into a Drude contribution and a mid-infrared band, both contributions exhibit a correlated increase as holes are transferred into the conducting CuO_2 planes and are therefore argued to be related to free carriers. We note that recent simulations of the t-J model, studied as a function of hole doping, provide a consistent description of such a behavior.

I. INTRODUCTION

One of the most intriguing features of the normal-state infrared spectrum of high-T_c superconductors is the extremely broad reflectivity spectrum extending up to the visible range that comprises a far-infrared, temperature-dependent response restricted roughly to the 0–1000-cm^{-1} range and a much broader contribution, extending up to 10 000 cm^{-1}, the so-called mid-infrared band (MIB), exhibiting a small (if any) temperature dependence. These features have been observed in very early studies and appear to be quite general in the high-T_c cuprates, e.g., $YBa_2Cu_3O_{6+x}$ (Refs. 1–6), $La_{1-x}Sr_xCuO_4$ (Refs. 7 and 8), or bismuth-related compounds (Refs. 9 and 10). They have given rise to various interpretations: one is the simultaneous occurrence of a Drude, temperature-dependent, far-infrared spectrum and a MIB bearing no particular relationship with the carriers.[1,2] Another suggestion is that the $YBa_2Cu_3O_7$ compound is not an ordinary Fermi liquid, relying essentially on a carrier-scattering rate exhibiting an unusual linear frequency dependence.[5,6] This latter dependence extends up to $\sim$2000 cm^{-1}; therefore no distinction is made in this analysis between a Drude and a mid-infrared contribution. A few quantitative studies have emphasized the variation on the effective carrier density that contributes to the optical conductivity up to a given frequency [$La_{1-x}Sr_xCuO_4$ (Ref. 8)] or the plasma frequency [$YBa_2Cu_3O_{6+x}$ (Ref. 4)] with doping. On the whole, few concentrations were available,[8] or eventually only defined through T_c.[4]

On the other hand, there is increasing experimental evidence that the simultaneous occurrence of both a Drude and a mid-infrared contribution is not a unique feature of the high-T_c cuprates. Indeed, optical studies of the doping effect in some metallic oxides (without copper) have shown that broad absorption bands appear as the materials are being doped[11–14] and, in some cases, seem to correlate with the free-carrier contribution.[13,14] Therefore, a systematic quantitative study of the infrared conductivity as a function of hole doping may help to sort out the specific characteristics, if any, of the mid-infrared absorption and of the Drude contribution in the high-T_c cuprates as compared to other metallic oxides, and to test some predictions of theoretical models.

Almost-localized-Fermi-liquid[15] approaches have addressed the doping dependence of the plasma frequency: it is essentially found that $\omega_p^2 \propto \delta$ (where δ is the hole concentration).[16,19] Some models predict the occurrence of a MIB whose spectral weight varies linearly with doping.[19]

Other descriptions of the normal state rely on an effective single-band Hubbard model, with a renormalized kinetic term t and a large on-site Coulomb repulsion energy U. This, in turn, yields the so-called t-J model, where $J = 4t^2/U$ is the characteristic energy for spin fluctuations.[20] The t-J Hamiltonian is believed to describe the electronic structure of the CuO_2 planes. At half-filling, namely when there are no holes, the system is insulating. The behavior of such systems at various doping levels is still under investigation. At very low doping [$\delta \to 0$] (Ref. 21)] the optical conductivity can be described by a quasiparticle band of width $2J$, which can be ascribed to the Drude peak, and an incoherent, much broader band of width $4t\sqrt{3}$, separated by a gap of the order of J. The optical properties of the one- and two-dimensional t-J models have been investigated through numerical simulations that seem to confirm this pic-

ture.[22,23] The validity of these arguments at higher doping levels does not appear to be firmly established.[24] The experimental data may be analyzed in the framework of such models.

In this paper we examine the behavior of the infrared reflectivity within two sets of samples from the 1:2:3 family, $YBa_2Cu_3O_{6+x}$ ($0 \le x \le 1$) and $Nd_{1+y}Ba_{2-y}Cu_3O_{6+x}$ ($0 \le y \le 0.5$), when changing the doping parameters x and y, in order to monitor the carrier concentration (and T_c) and to follow in a systematic way the possible relative changes in the reflectivity spectra that result from doping.

For the analysis, we have separated the reflectivity spectrum into a Drude contribution and a MIB. We show that in the metallic regime both these contributions can be assigned to holes present in CuO_2 conducting planes, and display the same doping dependence, strongly suggesting that they share the same physical origin. We discuss some possible counting arguments that describe the sequence of hole injection into the CuO_2 planes. Our results are in agreement with the conclusions drawn from x-ray absorption.[25] We finally compare our data to the predictions of the conductivity computed in the framework of the t-J model[21,22] and show that this model provides a consistent and quantitative description of our results.

II. EXPERIMENT

Well-controlled annealing conditions and precise knowledge of the oxygen content for $0 \le x \le 1$ are essential for this work. This is extremely difficult to achieve in the 1:2:3 single crystals. Indeed, there are few studies in the literature on such samples and most of the time the oxygen concentration is not actually known, so that just the critical temperature is mentioned.[3,4] It is not clear whether T_c is the proper criterion since it may not reflect the properties of the surface layer, of the order of 1000 Å, probed by the electromagnetic wave. Thin films would be ideal from this point of view; however, here again it is very hard to ascertain the oxygen content in a thin film. Oxygen control is eventually easier to achieve in bulk ceramic samples and one can check that the oxygen content is the same on the surface and in the bulk.[26] Therefore, we have decided to work on polycrystalline ceramic samples and perform the full analysis of their reflectivity spectrum, taking into account the various orientations of the single crystallites.[26] We have chosen well-characterized compounds, namely $YBa_2Cu_3O_{6+x}$ ($0 \le x \le 1$) and $Nd_{1+y}Ba_{2y}Cu_3O_{6+x}$ ($0 \le y \le 0.5$).

The behavior of the $YBa_2Cu_3O_{6+x}$ system has been extensively studied: it is well known to be insulating at $x=0$, and that as one fills up the oxygen vacancies within the chains the system becomes metallic and superconducting around $x=0.4$. $YBa_2Cu_3O_{6+x}$ ceramic disks (12 mm diameter, 2 mm thick) have been prepared by a standard solid-state reaction technique[27]; their oxygen content has been determined by the weight change after controlled annealing under oxygen partial pressure.[27]

The $Nd_{1+y}Ba_{2-y}Cu_3O_{6+x}$ ($0 \le y \le 0.5$) materials have also generated much interest.[28–31] Our compounds have been prepared by a standard ceramic technique. Their transition temperatures are the same as found earlier in these compounds.[28,29] It was shown that the Nd^{3+} in excess goes into the Ba^{2+} site.[32] The extra oxygen atoms ($x > 1$) are thought to go into sites near Cu(1) along the a axis, which are left vacant in $YBa_2Cu_3O_7$, leading eventually to an orthorhombic-to-tetragonal transition at $y \sim 0.2$.[28,29] Iodometric titration allows us to determine the effective Cu^{3+} concentration or, rather, the effective charge p of $[Cu\text{-}O]^p$.[31,33] We have performed such iodometric titration on our samples. As in earlier work, we find p independent of y, and equal to 0.25 ± 0.03. From charge neutrality considerations, this implies that the oxygen content x increases with y. We find that x goes from 0.88 up to 1.08 as y goes from 0 to 0.4. Starting from $y=0$ ($x \sim 0.88$) and increasing y, the critical temperature decreases, consistently with earlier work.[28] At large y (≥ 0.4), the system exhibits semiconducting behavior, albeit with a sharp resistivity decrease at 4 K. This behavior fits into the general phase diagram of Tokura *et al.*,[33] showing that according to the x and p values one may obtain either an insulating or a superconducting sample. What appears to be the relevant quantity to characterize the metallic regime is $p - p_0$, where p_0 is a threshold value that depends linearly on x.[33]

Reflectivity spectra have been recorded at room temperature in the 500–25 000-cm^{-1} range in two steps, using an infrared IFS 66 Bruker spectrometer between 500 and 7000 cm^{-1} and a visible Cary 17 spectrometer in the range 5000–25 000 cm^{-1}. Our ceramics have been mechanically polished in order to achieve a mirrorlike surface and we have chosen a silver mirror as a 100% reflectivity reference. In earlier optical investigations on polycrystalline samples, the surface reference was the ceramic itself, coated with evaporated gold or silver,[1,34] the assumption being that this normalization takes into account diffusion due to the surface roughness. When doing so, one replaces a surface with a given roughness related to the granular structure of the ceramic, that is—more or less randomly oriented anisotropic crystallites—by a surface exhibiting presumably the same geometrical roughness, now coated, however, with an isotropic material. We have also tried to perform such coatings, and we have noticed strong irrelevant features in the so-called reference spectrum. Our normalization allows for uncertainties due to light diffusion by the residual roughness. Typically, the loss of specular reflected light is of the order of 5%. Corrections have been carefully studied and applied in order to minimize such errors.[35] Most important is the fact that these uncertainties cannot alter the trends that emerge from the evolution of the spectra as a function of doping.

III. RESULTS AND ANALYSIS

Reflectivity spectra for both sets of samples at normal incidence are displayed in Fig. 1, in the 1000–20 000-cm^{-1} range, for a limited number of x and y values. The largest changes as a function of x or y occur in the infrared range. In the following, both spectra exhibit the same qualitative trends.

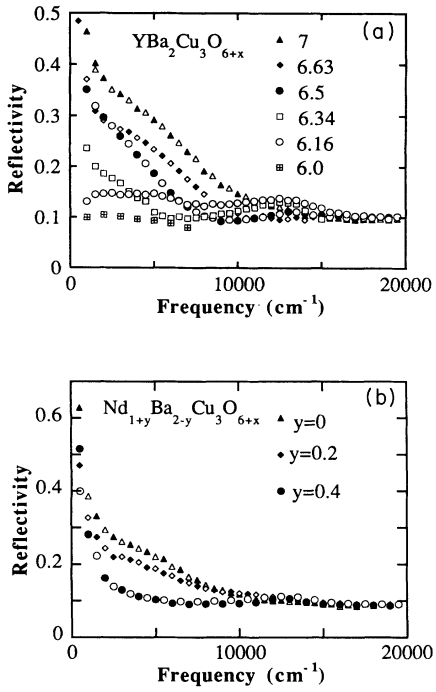

FIG. 1. Reflectivity spectra of (a) $YBa_2Cu_3O_{6+x}$ $(0<x<1)$ and (b) $Nd_{1+y}Ba_{2-y}Cu_3O_{6+x}$ $(0<y<0.5)$ for selected values of x and y. The solid symbols are the experimental points; the open symbols are the fitted points when appearing together with the solid symbols.

In the case of the $YBa_2Cu_3O_{6+x}$ family, Fig. 1(a), there is no infrared response (except for phonon structures, not shown here since they lie below 1000 cm^{-1}) in the undoped (insulating) sample $YBa_2Cu_3O_6$. A broad infrared feature emerges below 10 000 cm^{-1} as soon as the system is doped ($x=0.16$) and appears to shift towards lower energies as x increases (0.28, 0.34). Above $x=0.5$ (not shown), a far-infrared response develops, as testified by the rise below 1500 cm^{-1}.

In the case of $Nd_{1+y}Ba_{2-y}Cu_3O_{6+x}$, a similar behavior is observed [Fig. 1(b)] when decreasing y from 0.5 to 0, which is the analog of increasing x in the former set of samples: the mid-infrared spectrum increases gradually, and the far-infrared sharp rise is most clearly seen. We recall that in this case the oxygen content x changes very little (0.88–1.08) and, in particular, the chains start from an almost entirely saturated situation ($x=0.88$).

A quantitative analysis is not straightforward; since the electric field does not lie along any principal axis of the system, no Kramers-Kronig (KK) transform may be achieved. In order to extract the parameters that yield the optical conductivity associated with the *ab* plane, we must fit the reflectivity spectrum directly. The details of the analysis that apply to polycrystalline samples have been published elsewhere.[26] The starting point is that the reflected flux is a sum over all contributions of randomly oriented crystallites:

$$R=\tfrac{1}{2}(R_o+\langle R_e\rangle)\,, \tag{1}$$

where R_o is the reflectivity for the ordinary wave, with the electric field lying in the *ab* plane, and $\langle R_e\rangle$ is an angular average of the reflectivity of the extraordinary wave.[4,26] R_o and R_e can be computed using the dielectric constants relevant to the principal axes. Because of twinning, we take $\epsilon_a=\epsilon_b=\epsilon_{ab}\neq\epsilon_c$. Such an analysis should hold as long as the wavelength of the electromagnetic wave remains small compared to the size of the elementary crystallite. We have studied a number of reflectivity spectra on various samples exhibiting different grain sizes, from typically 20 μm down to less than 1 μm. Differences which are expected to occur between the reflectivity spectra at different wavelengths according to the grain size on account of the above argument have been found to be negligible down to 500 cm^{-1}, e.g., a 20-μm wavelength.

It has been argued that the *ab*-plane optical conductivity in the infrared range (up to 10 000 cm^{-1}) can be described by a Drude contribution and a MIB around 2000–4000 cm^{-1}.[1–4] We shall make use of this description as a convenient phenomenology in order to analyze the behavior of these two parts of the spectrum. The infrared response in the *ab* plane can be described by the following dielectric constant:

$$\epsilon_{ab}(\omega)=\epsilon_\infty-\omega_p^2/[\omega(\omega-i\tau^{-1})]+\omega_f^2/(\omega_0^2-\omega^2+i\omega\gamma)\,. \tag{2}$$

ϵ_∞ is the dielectric constant that accounts for the high-frequency contributions. The Drude part is represented by the plasma frequency ω_p, and $1/\tau$ is the carrier-scattering rate; the MIB has a central frequency ω_0, an oscillator strength ω_f, and a width γ. Visible-band contributions that do not appear in (2) have been included in the fit and will be discussed elsewhere.[35] We also assume that there may exist a plasma frequency ω_c, but that there is no MIB along the *c* direction, whatever x or y, in agreement with earlier observations.[36–38]

In the $0<x<0.34$ range, the MIB cannot actually be represented by a single oscillator. Indeed, Fig. 1 shows some structure in the reflectivity for $x=0.16$. We have plotted in Fig. 2 the central frequencies for these bands. Both show the same behavior, namely their frequency shift towards lower energies as x increases. Above $x=0.34$, satisfactory fits can be achieved with a single MIB and we do not find any further change of its frequency, as can be seen in Fig. 2. Although there are no

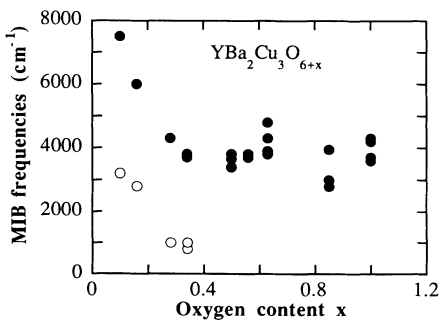

FIG. 2. Variation of the MIB central frequency with x in $YBa_2Cu_3O_{6+x}$ $(0<x<1)$. The solid symbols represent the main MIB, the open ones the secondary band (see text).

quantitative estimates in the literature, from the various conductivities shown in $YBa_2Cu_3O_{6+x}$, as well as in $La_{2-x}Sr_xCuO_4$,[4,8] it seems that the MIB shifts towards lower energies as doping increases. We cannot rule out this possibility, but we cannot confirm it either, most likely because the range of acceptable parameters is in our case too large to allow a precise determination of this quantity.

Indeed, several sets of parameters yield similar satisfactory fits; one example is shown in Figs. 1(a) and 1(b). A computed reflectivity spectrum is considered to fit satisfactorily if it deviates by less than $\pm 3\%$ from the experimental spectrum. We do not consider computed spectra, which, although acceptable with respect to the above criterion, exhibit a systematically higher or lower slope $dR/d\omega$ than the experimental one. In other words, we accept local differences of $\sim 3\%$ but not overall deviations. We have also rejected the sets of ω_p and ω_c, values which, though providing satisfactory fits, yield a dc conductivity ratio $\sigma_{ab}/\sigma_c < 10$. According to resistivity measurements,[36] $\sigma_{ab}/\sigma_c \sim 30$; we thus allow, somewhat arbitrarily, a factor of 3 for the relaxation-time anisotropy.

Actually, changing the reflectivity by $\pm 3\%$ is not the major source of uncertainty. What heavily undermines the accuracy of the parameters is the fact that the Drude and the MIB overlap at high doping levels. One can decrease ω_p and balance this decrease by increasing the weight ω_f of the MIB and, conversely, without significantly changing the shape of the spectrum. The range of variation of ω_p and ω_f decreases for the lowest x values when the overlap gets smaller. In this paper, we do not discuss in further detail the various parameters extracted from the fits and their range of variation. This range will be displayed by the scatter of the experimental points for a given (x or y) concentration in the various forthcoming plots (Figs. 4–9). In the case of the $Nd_{1+y}Ba_{2-y}Cu_3O_{6+x}$ system, we put in some extra error bars due to the lower quality of the polished surface.

Each set of parameters allows one to compute an optical conductivity associated with the *ab* plane. We show in Fig. 3 such typical conductivities for selected x and y values. The MIB is apparent on all spectra, because of its large weight and fairly high central frequency. The conductivities that we deduce do not quantitatively map the conductivities obtained from reflectivity data on single crystals through a KK transform.[4] Recall, however, that in our fitting procedure we have described the MIB by a single Lorentz oscillator up to 12 000 cm^{-1}, e.g., in the whole infrared range. In contrast, the KK transform does not call for a model for the line shape of the MIB. This is certainly a major drawback of working on ceramic samples. It is nevertheless obvious that, as the doping is changed, the trends observed in Fig. 3 are similar to those observed on single crystals.

The sum rule restricted to the Drude conductivity σ_D yields the plasma frequency

$$\int_0^{+\infty} \sigma_D(\omega) d\omega = \frac{\omega_p^2}{8} . \tag{3}$$

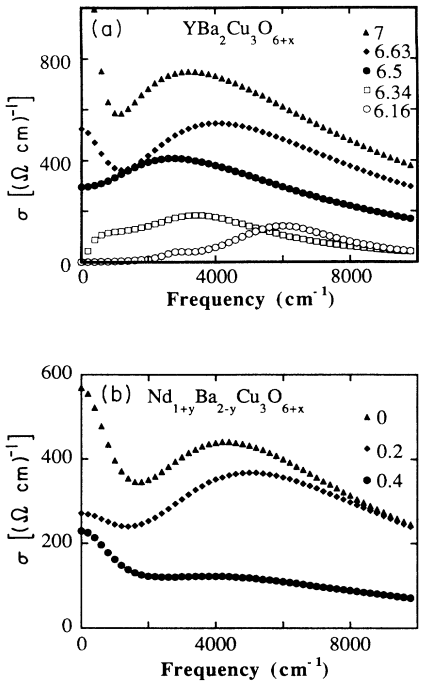

FIG. 3. Computed (*ab*) plane conductivity spectra for the same x and y values as shown in Fig. 1.

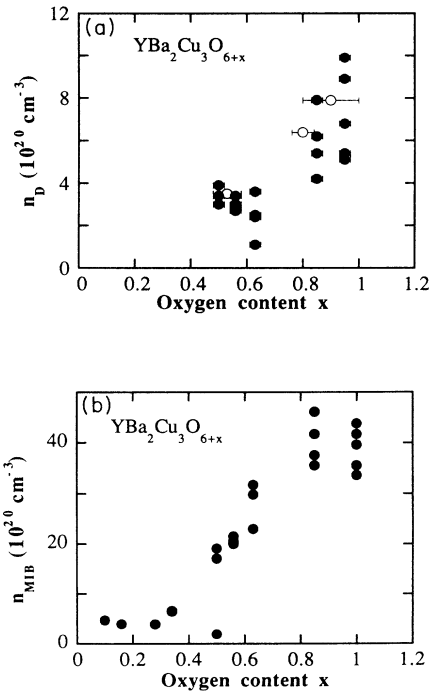

FIG. 4. Variation of the Drude and MIB effective carrier densities in $YBa_2Cu_3O_{6+x}$ ($0 < x < 1$). Error bars on the oxygen content are only shown in the upper panel. The open symbols are from Ref. 4, normalized by a factor of ~ 2 (see text). The scatter of the points for a given x value represents the possible values of the parameters that fit the reflectivity equally well (see text). As a rule of thumb, the larger n_D is, the smaller n_{MIB} is.

For simplicity, we extracted from the plasma-frequency value a carrier density n_D, taking for m the free-electron mass. n_D thus represents the free-hole density in the Drude model and may be directly compared to ω_p^2.

A similar integral can be written for the MIB conductivity σ_{MIB}, which readily yields the density of localized oscillators, n_{MIB}, associated with the MIB in the framework of the classical model of a Lorentz oscillator being used here.[4] Such oscillators may be viewed as localized holes since they do not contribute to the zero-frequency conductivity.

Figures 4 and 5 show n_D and n_{MIB} for $YBa_2Cu_3O_{6+x}$ and $Nd_{1+y}Ba_{2-y}Cu_3O_{6+x}$, respectively.

n_D exhibits a large dispersion, especially at $x \sim 1$ in $YBa_2Cu_3O_{6+x}$ [Fig. 4(a)]. This is mainly due to the fact that the overlap of the two components is the largest at this concentration and the decomposition is somewhat arbitrary. Orenstein *et al.* have measured the plasma frequency for three single crystals exhibiting different T_c. Their values are larger than ours, by approximately a factor of 1.4. (A review of the measured plasma frequencies in $YBa_2Cu_3O_7$ indeed shows a fairly large dispersion of the experimental values.[1] As a matter of comparison, we have inserted in Fig. 4(a) the three values found in Ref. 4, normalized to ours. The relative variation of both sets of data is fully compatible.

n_{MIB} is stable and of the order of 4×10^{20} cm^{-3} for $x<0.34$ (n_{MIB} comprises, in this case, the two bands); it then shows a break around $x=0.34$, above which the onset of the Drude contribution occurs, and goes up by almost an order of magnitude [Fig. 4(b)].

For $Nd_{1+y}Ba_{2-y}Cu_3O_{6+x}$ (Fig. 5), the behavior is qualitatively the same for y decreasing from 0.5 to 0 as for $x>0.34$.

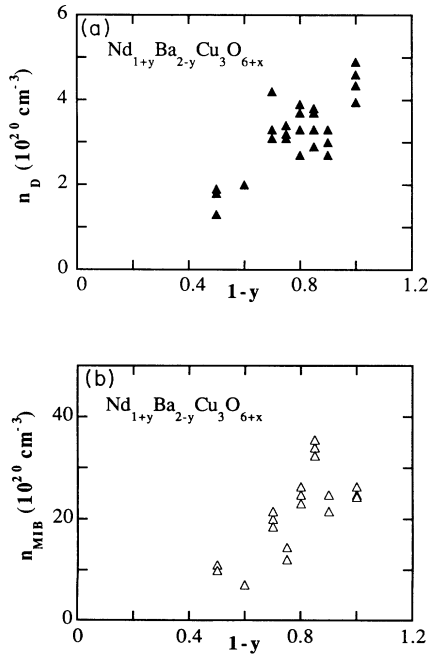

FIG. 5. Variation of the Drude and MIB effective carrier densities in $Nd_{1+y}Ba_{2-y}Cu_3O_{6+x}$. The scatter of the points for a given x value represents the possible values of the parameters that fit the reflectivity equally well.

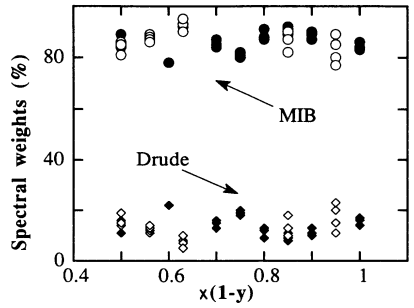

FIG. 6. Relative spectral weights of the Drude and MIB components in the $YBa_2Cu_3O_{6+x}$ ($0<x<1$) (open symbols) and $Nd_{1+y}Ba_{2-y}Cu_3O_{6+x}$ ($0<y<0.5$) (solid symbols).

In both compounds, the hole densities n_D and n_{MIB} seem to grow simultaneously with doping. We have plotted in Fig. 6 the ratios $n_D/(n_D+n_{\mathrm{MIB}})$ and $n_{\mathrm{MIB}}/(n_D+n_{\mathrm{MIB}})$ for both sets of samples: they exhibit quantitatively the same behavior, namely the relative weights of the Drude and MIB contributions remain constant (to within our experimental accuracy) as their absolute weights increase.

IV. DISCUSSION OF HOLE DISTRIBUTION

Hole counting versus doping and their respective distribution between planes and chains has been performed in various ways. We do not discuss Hall measurements since the temperature dependence of the Hall coefficient suggests that it may not be simply related to the free-carrier density. We shall compare our optical results to those of chemical titration[30,31] and x-ray absorption.[25] These two techniques address the problem of hole counting without making any distinction between possible free and localized carriers.

For the matter of the comparison, we must implement our analysis in order to account for all the holes that are introduced by doping. To do so, we have computed the full integrated conductivity:

$$\int_0^{+\infty}[\sigma_D(\omega)+\sigma_{\mathrm{MIB}}(\omega)]d\omega=\frac{\pi N_{\mathrm{tot}}e^2}{2m^*} . \tag{4}$$

The variation of N_{tot}, which is the relevant quantity to be compared to chemical titration or x-ray absorption results, is shown in Fig. 7.

N_{tot} looks similar to the Cu $3d$ hole count at the Cu(1) site evaluated by x-ray-absorption spectroscopy on $YBa_2Cu_3O_{6+x}$.[25] Both quantities exhibit a plateau below $x\sim0.34$ and an increase above this concentration. The data of Fig. 4(a) show the onset of the Drude term above $x=0.34$: such free carriers are unlikely to occur within the chains because any defect is able to prevent one-dimensional (1D) conduction. Therefore we assign the occurrence of the Drude term to free holes in the CuO_2 planes. This interpretation is corroborated by the increase of the value of the Drude term n_D with decreasing

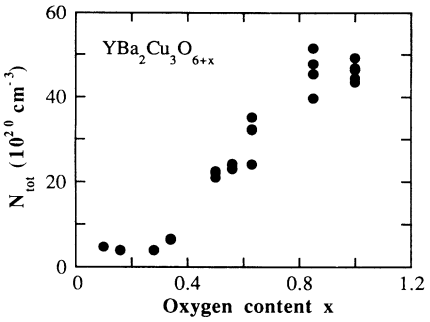

FIG. 7. Total hole density associated with oxygen uptake in $YBa_2Cu_3O_{6+x}$.

y in $Nd_{1+y}Ba_{2-y}Cu_3O_{6+x}$ [Fig. 2(b)], which compares quantitatively with $YBa_2Cu_3O_{6+x}$ data with increasing x. In this case, the increase of n_D cannot be related to the chains from which oxygen is actually removed with decreasing y. Indeed, in this system, the only possibility is that the hole-density variation occurs within the planes. ^{63}Cu zero-field NMR data are also available as a function of x and provide compelling indications that mobile holes appear in the CuO_2 planes at $x \sim 0.3$.[39]

The increase of hole density at $x > 0.34$ is associated with the sharp growth of the weight of the MIB for the same concentration (Fig. 4), which develops with x along with the weight of the Drude term (Fig. 6). This fact suggests that in the metallic regime the MIB and the Drude term share the same origin, e.g., the occurrence of free carriers in the CuO_2 planes.

At $x < 0.4$, N_{tot} must be entirely assigned to the MIB. Both the MIB frequency shift for $0 < x < 0.34$ (Fig. 2) and the sharp increase of its oscillator strength at $x \sim 0.34$ [Fig. 4(b)] suggest that, in the insulating phase and in the metallic phase, the MIB does not have the same origin.

In the insulator, we assign N_{tot} to localized holes appearing within the chains. For $x < 0.2$, according to the x-ray-absorption data, each oxygen atom gives rise to two Cu^{2+} ions[25] meaning that Cu^{2+}-O^{2-}-Cu^{2+} entities are building up. In these data the plateau above $x \sim 0.2$ is interpreted in terms of the lengthening of these small chains, with holes being put into the O $2p$ orbitals. We then speculate that such chains of variable length provide a spatially limited path for this hole, which couples to the electromagnetic field. As the chain gets longer, the hole becomes less localized. In a Lorentz-oscillator scheme, this means that the restoring force gets smaller, and so does the frequency of this oscillator, as observed. Also, since it is not the number of O-Cu-O chains that increases, but the lengths, the oscillator strength does not change.

Our results can also be compared to chemical titration data. In the $Nd_{1+y}Ba_{2-y}Cu_3O_{6+x}$ case, it was suggested that, in order to explain the increasing conductivity (and higher T_c) of samples otherwise exhibiting constant effective charge per copper p, the free-carrier density is instead only related to the holes in the CuO_2 planes, $p_{pl} = \frac{3}{2}(p - p_0)$. p_{pl} is the charge per copper atom within one CuO_2 plane. $3p_0$ is a saturation hole density that the chains can accommodate (Ref. 33). p_0 is found empirically to increase linearly with the oxygen content x as $p_0 = (x - x_0)/3$, where $x_0 \sim 0.5$.[33] Since as y increases, x and p_0 also increase, more holes are therefore localized on the chains and less are available in the planes, at constant p.

We may compare the free-carrier density corresponding to p_{pl}, resulting from chemical titration, to both p_{tot} deduced from N_{tot} (assuming for m^* the free-electron mass m_0) and to p_D deduced from n_D (introducing a renormalized mass m^*). For $YBa_2Cu_3O_{6+x}$, p_{pl} is just computed from x using $3p = 2x - 1$ and $p_{pl} = \frac{3}{2}(p - p_0)$; hence $p_{pl} = \frac{1}{2}(x - 1 + x_0)$. For $Nd_{1+y}Ba_{2-y}Cu_3O_{6+x}$, we have used the experimentally determined p values in order to deduce p_{pl} as in Ref. 33. In both cases, we have taken $p_0 = 0.45 \pm 0.05$. These comparative plots are shown in Figs. 8 and 9.

The linear relationship between p_{pl} and x does not hold for p_{tot} as determined by optics in the case of $YBa_2Cu_3O_{6+x}$, whereas the discrepancy is not obvious in the $Nd_{1+y}Ba_{2-y}Cu_3O_{6+x}$ data, due to the fairly large dispersion of the points. Interestingly enough though, the magnitudes of p_{pl} and p_{tot} are consistent, taking for m^* the bare electron mass m_0. In order to adjust the Drude contribution p_D at the p_{pl} values, we have to introduce an effective mass: In Figs. 8(b) and 9(b), we have chosen $m^* = 4m_0$. Since the dispersion of the data is larger on n_D than on N_{tot}, the discrepancy observed in Fig. 8(b) between p_{pl} and p_{tot} is now less obvious concerning p_{pl} and p_D in the case of $YBa_2Cu_3O_{6+x}$. However, we note in Fig. 8(b), as in Fig. 8(a), that the low-x data (0.56 and 0.5) are systematically above the straight line defined by p_{pl}. In contrast, the $Nd_{1+y}Ba_{2-y}Cu_3O_{6+x}$ p_D

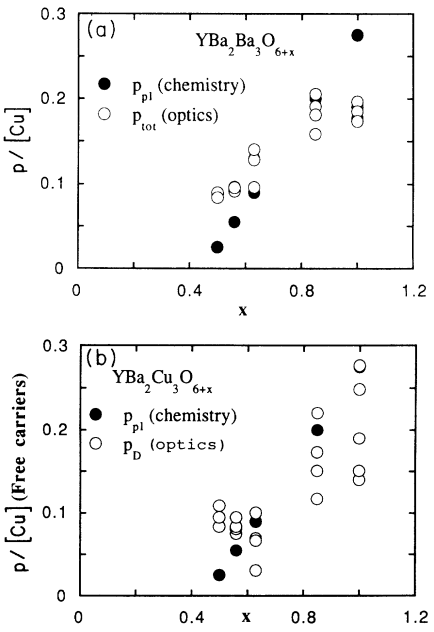

FIG. 8. Comparison of $p_{pl} = \frac{3}{2}(p - p_0)$ determined by charge neutrality considerations with (a) p_{tot} and (b) p_D in $YBa_2Cu_3O_{6+x}$ $(0.4 < x < 1)$ (see text).

data are reasonably consistent with p_{pl} [Fig. 9(b)].

Let us also examine the possible consequences of this description if we now assign the MIB to holes along the chains. One would then expect that, as the Drude term grows, the MIB decreases in order to reflect the balance of the total effective charge. This is completely in opposition to our findings. Despite the fact that there must be some distribution of the effective charge between localized and free carriers, we do not find any detectable signature of the localized holes in the metallic regime. Moreover, p_{pl} appears to be more consistent with p_{tot} than with p_D, therefore calling for the MIB contribution. These results clearly show that the MIB correlates with the free-carrier density in the CuO_2 planes.

One might still object, as far as the MIB is concerned, that in untwinned $YBa_2Cu_3O_7$ single crystals the conductivity σ_b along the b (chain) direction is found to be significantly higher than along the a direction (σ_a), where only the CuO_2 planes are being probed.[5,6] How much of the σ_b conductivity should be attributed to the chains is, however, not straightforward. Indeed, because of possible disorder, "chain conductivity" may require short deviating paths parallel to the c axis connecting the chains through the planes. Therefore "chain" and "plane" conductivities may not simply add up. Besides, whether the ratio σ_b/σ_a does not change for lower oxygen contents remains to be established. We note that in the $La_{2-x}Sr_xCuO_4$ single crystal[8] (no chains) the Drude and MIB components are present with a relative weight similar to what we find. An attempt was indeed made to separate these two contributions of the infrared spectrum. It was found that the weight of the Drude component was 10 times smaller than the overall infrared spectral weight, a figure which compares with our findings (Fig. 6). Finally, our own observations show that the MIB behavior in both $YBa_2Cu_3O_{6+x}$ ($0.34<x<1$) and $Nd_{1+y}Ba_{2-y}Cu_3O_{6+x}$ ($0<y<0.4$) compounds is strikingly similar, whereas the chain configuration is completely different as doping occurs; hence one might expect the chain contribution to conductivity to be quite different. As an example, Figs. 4(b) and 5(b) show that in two samples having the same T_c (~ 50 K), whether the chains are half-filled ($x=0.5$) or completely filled ($y=0.2$, $x\sim 1$), n_{MIB} is typically the same ($\sim 2\times 10^{21}$ cm^{-3}). Therefore, we believe the actual chain contribution to be negligible compared to the plane contributions and we conclude that the MIB is correlated with carriers in the CuO_2 planes.

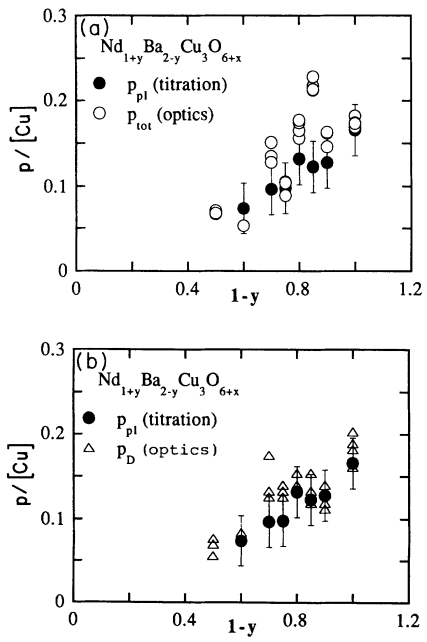

FIG. 9. Comparison of $p_{pl}=\frac{3}{2}(p-p_0)$ (p being determined by iodemetric titration) with (a) p_{tot} and (b) p_D in $Nd_{1+y}Ba_{2-y}Cu_3O_{6+x}$.

V. MODELIZATION OF THE OPTICAL CONDUCTIVITY

Few Fermi-liquid models address the question of the MIB. Kotliar *et al.* find an interband transition, which they expect to be very broad and whose oscillator strength is proportional to the hole concentration δ.[16] However, the oscillator strengths of the Drude term and of this interband transition should be comparable, which is in sharp contrast with the measurements. The linear dependence of ω_p^2 with δ (Refs. 16–19) does not seem to apply to our data: this linear behavior translates in our plot into a linear behavior of n_D versus x or $1-y$. The straight line should extrapolate roughly at the doping value $x_0\sim 0.4$ or $y_0\sim 0.5$, which corresponds to $\delta=0$. We find instead $x_0=0.3\pm 0.1$ and $y_0=0.6\pm 0.1$, a systematic deviation from the expected values. One could argue that considering the dispersion of the points it is not unlikely that one can draw a straight line ending up at $x_0=0.4$ and $y_0=0.5$. However, one should note that upon doing so one systematically leaves out the $x<0.55$ and $y>0.25$ data, as also shown in Fig. 8(b). Although our estimates of the plasma frequencies are smaller than those of Ref. 4, the behavior of ω_p^2 versus x is similar: a straight line would extrapolate at $x\sim 0.25$. In fact, close to the metal-insulator transition, n_D seems to rise abruptly.

We now briefly discuss the simultaneous growth of the two contributions in the framework of a band model. The possibility of an interband transition whose initial or final states could be the Fermi level and, hence, whose intensity would reflect the density of states at the Fermi level, cannot be ruled out, due to the huge complexity of any band model. However, calculations of the optical conductivity show a much lower conductivity below 0.5 eV than around 2 eV, which is contrary to the experimental data.[40]

Some recent experimental data on nonsuperconducting materials (metallic oxides) that exhibit similar though not identical features, namely a Drude peak and a MIB, might suggest that the origin of the MIB is still unclear, namely:

(i) In $La_{2-x}Sr_xNiO_4$, a MIB is observed for $x=0.2$ and none for $x=0$, but nothing could be said about the relative weights of the Drude and the MIB.[2]

(ii) In the metallic cubic oxide $Nd_{1-x}Sr_xCoO_3$, one also observes the simultaneous growth of a Drude peak and of a MIB.[13] The authors of Ref. 13 note a number of qualitative differences with cuprate superconductors that they attribute at least partially to differences between Co^{3+} and Cu^{2+} states. The MIB by itself may not be specific to the cuprates. However, it might display unique characteristics deserving further analysis.

We organize a more quantitative discussion by analyzing our results in the framework of the 2D Hubbard model and the derived t-J model.[5,6,21,22]

These models describe the electronic structure of CuO_2 planes. In absence of doping, the ground state exhibits long-range antiferromagnetic order. With hole doping, this state is destroyed and it is believed that the resonating valence bond state is the actual ground state.[41] This is the case that should be applicable to our experimental situation, since antiferromagnetic order has disappeared in $YBa_2Cu_3O_{6+x}$ at $x \sim 0.4$ when holes are introduced into the CuO_2 planes and also for any y ($0 \leq y \leq 0.4$) in $Nd_{1+y}Ba_{2-y}Cu_3O_{6+x}$. We also note that the smallest energy scale of the $\epsilon_p - \epsilon_d$ model lies above our energy range (less than 1.5 eV), so that the model reasonably applies to the experimental situation.

The motion of a hole in an antiferromagnet is discussed first in the limit of $J_z \neq 0$ and $J_\perp = 0$ and yields a set of bound states. The effect of introducing $J_\perp$ discriminates between these states, giving rise to a continuum of width $4t\sqrt{3}$ and to a set of coherent peaks ranging over $2J_\perp$ in energy. These two components are separated by a gap of the order of J_z.

In this framework, the optical conductivity behaves as follows.

(a) For $n_h = 0$ (no hole doping), no infrared conductivity is expected. Only the upper Hubbard band is present, leading to absorption at energy of the order of U.

(b) With hole doping, spectral weight is transferred to the low-energy range. The coherent peaks can be ascribed to the Drude peak (hence $1/\tau = J_\perp$), separated by the gap (J_z) from an incoherent background with a total width of $4t\sqrt{3}$, which stands for the MIB (hence $\gamma = 2t\sqrt{3}$).

(c) As doping increases, the MIB is found to shift towards lower energies.

(d) The spectral weight of the quasiparticle peak is of the order of J_z/t, and the quasiparticle effective mass is enhanced by a $t/J_\perp$ factor.

The fact that both the Drude peak and the MIB develop together with doping, as illustrated in Figs. 2 and 4, is a natural consequence of the model, since one just adds the independent contributions of the holes. In such a case, the relevant quantity needed to represent the hole concentration is $N_{\rm tot}$, plotted in Fig. 7. The t-J model yields the conductivity changes that have been observed in $La_{2-x}Sr_xCuO_4$, where there is an obvious spectral weight transfer from the high-energy part of the spectrum towards the low-energy part.[8] The shift of the MIB with doping also appears in conductivity spectra already published.[4,8] We ourselves have no evidence of such a frequency shift towards low energies with doping, but we already mentioned the uncertainty in this determination.

We turn to quantitative estimates of t and J through our own data. The values we find for t, $J_\perp$, and J_z are deduced from the respective widths of the MIB (t), Drude peak ($J_\perp$), and the relative spectral weight of the Drude peak (J_z).

We find, for $YBa_2Cu_3O_{6+x}$ and $Nd_{1+y}Ba_{2-y}Cu_3O_{6+x}$,

$$J_\perp = 0.13 \pm 0.06 \text{ and } 0.13 \pm 0.06 \text{ eV},$$

$$t = 0.31 \pm 0.02 \text{ and } 0.37 \pm 0.03 \text{ eV},$$

$$J_z = 0.08 \pm 0.03 \text{ and } 0.10 \pm 0.04 \text{ eV},$$

irrespective of x and y.

$J_z \sim J_\perp = J$, as it should, though both terms are extracted from independent data. The upper values are reasonable figures for t and J.[21,22] They also compare reasonably with the current values for t (0.2–1 eV) and $J = 4t^2/U$ (0.02–0.25 eV). The mass enhancement deduced is 4 ± 2, in agreement with earlier data.[5,6] These results show that the t-J model provides a consistent description of the normal state.

Schlesinger *et al.* have recently suggested that the Fermi-liquid picture cannot fully account for the unusual linear frequency dependence of the scattering rate $1/\tau$.[5,6] Indeed, the correlated increase of the Drude and MIB components and the relative independence of ω_p^2 with hole concentration n_h are features that emerge more naturally in a non-Fermi-liquid picture.[42–44]

VI. CONCLUSIONS

We have shown that for the case of hole doping the total infrared response should be taken into account. This, together with the quantitative comparison of two different sets of differently doped samples, shows that the so-called MIB and the Drude term share the same origin, e.g., the occurrence of free carriers in the CuO_2 planes.

Our findings eventually suggest the desirability of more precise quantitative analysis of the optical data, in the high-T_c cuprates as well as in nonsuperconducting noncuprates, and, in particular, more careful analyses of the plasma frequency, of the characteristic frequency of the MIB, and of the respective weights of the two components versus doping.

ACKNOWLEDGMENTS

We are grateful to Professor R. Combescot for illuminating discussions. Laboratoire d'Optique Physique is Unite Associeé No. 0005 du Centre National de la Recherche Scientifique.

*Permanent address: Laboratoire de Physique de la Matière Condensée, Ecole Normale Supérieure, 24 rue Lhomond, 75231 Paris CEDEX 05, France.

[1]For a review, see T. Timusk and D. B. Tanner, in *Physical Properties of High T_c Superconductors,* edited by D. M. Ginsberg (World Scientific, Singapore, 1989).
[2]T. Timusk *et al.*, Physica C **162-164**, 841 (1989).
[3]S. L. Cooper *et al.*, Phys. Rev. B **40**, 11 358 (1989).
[4]J. Orenstein *et al.*, Phys. Rev. B **42**, 6342 (1990); J. Orenstein and D. H. Rapkine, Phys. Rev. Lett. **60**, 968 (1988).
[5]Z. Schlesinger *et al.*, Phys. Rev. B **41**, 11 237 (1990).
[6]Z. Schlesinger *et al.*, Phys. Rev. Lett. **65**, 801 (1990).
[7]S. Uchida *et al.*, Physica C **162-164**, 1677 (1989).
[8]S. Uchida *et al.*, Phys. Rev. B **43**, 7942 (1991).
[9]I. Terasaki *et al.*, Physica C **165**, 152 (1990).
[10]J. Bouvier *et al.*, J. Less-Common Met. **164-165**, 1092 (1990).
[11]Z. Schlesinger *et al.*, Phys. Rev. B **40**, 6862 (1989).
[12]Xiang-Xin Bi *et al.*, Phys. Rev. B **42**, 4756 (1990).
[13]I. Terasaki *et al.*, Phys. Rev. B **43**, 551 (1991).
[14]Y. Watanabe *et al.*, Phys. Rev. B **43**, 3026 (1991).
[15]For a review of the Fermi-liquid approaches, see K. Levin *et al.*, Physica C **175**, 449 (1991).
[16]G. Kotliar *et al.*, Physica C **153-155**, 538 (1988).
[17]J. H. Kim *et al.*, Phys. Rev. B **40**, 11 378 (1989).
[18]M. Grilli *et al.*, Phys. Rev. B **42**, 329 (1990).
[19]P. A. Lee *et al.*, Physica B **148**, 274 (1987).
[20]F. C. Zhang *et al.*, Phys. Rev. B **37**, 3759 (1988).
[21]C. L. Kane *et al.*, Phys. Rev. B **39**, 6880 (1989).
[22]W. Stephan *et al.*, Phys. Rev. B **42**, 8736 (1990).
[23]D. Poilblanc *et al.*, Phys. Rev. B **44**, 9562 (1991).
[24]W. Stephan *et al.*, Phys. Rev. Lett. **66**, 2258 (1991).
[25]H. Tolentino *et al.* (unpublished).
[26]N. Bontemps *et al.*, J. Phys. (Paris) **50**, 2895 (1989).
[27]P. Monod *et al.*, J. Phys. (Paris) **48**, 1369 (1987).
[28]K. Takita *et al.*, Jpn. J. Appl. Phys. **27**, L57 (1988).
[29]K. Takita *et al.*, Jpn. J. Appl. Phys. **27**, L607 (1988).
[30]M. W. Shafer *et al.*, Phys. Rev. B **39**, 2914 (1989).
[31]M. W. Shafer *et al.* (unpublished).
[32]F. Izumi *et al.*, Jpn. J. Appl. Phys. **26**, L1616 (1987).
[33]Y. Tokura *et al.*, Phys. Rev. B **38**, 7156 (1988).
[34]S. G. Kaplan *et al.*, Phys. Rev. B **38**, 5006 (1988).
[35]J. Bouvier, Ph.D. thesis, University of Paris, 1991.
[36]T. Penney *et al.*, Phys. Rev. B **38**, 2918 (1988).
[37]A. V. Bazhenov *et al.*, Physica C **162-164**, 1247 (1989).
[38]I. Bozovic *et al.*, Phys. Rev. B **38**, 5077 (1988).
[39]P. Mendels *et al.*, Physica C **171**, 42 (1990).
[40]Guang-Lin Zhao *et al.*, Phys. Rev. B **36**, 7203 (1987).
[41]P. W. Anderson, Science **35**, 1196 (1987).
[42]P. W. Anderson *et al.*, Phys. Rev. Lett. **60**, 132 (1988).
[43]N. Nagaosa *et al.*, Phys. Rev. Lett. **64**, 2450 (1990).
[44]J. P. Rodriguez, Phys. Rev. B **44**, 9582 (1991).